ETWatch: a method of multi-resolution ET data fusion

LIU Shufu, XIONG Jun, WU Bingfang

Institute of Remote Sensing Applications, Chinese Academy of Sciences, Beijing 100101*, China*

Abstract: Construction of a high-resolution remote-sensing evapotranspiration (ET) dataset is restricted by remote sensing data sources and clouds. Single remote sensor data cannot cover the land with high spatial and temporal resolution. In this paper, we analyzed the spatial characteristics of different scale ET data in ETWatch, compared several common fusion methods, and analyzed the data characteristics and information before and after data fusion. We integrated the spatial and temporal adaptive reflectance fusion model (STARFM) into ETWatch to fuse different scale remote sensing ET data. The results show that the STARFM fusion method effectively can integrate the spatial and temporal distribution information of high & low resolution data, with an average error of 1.75%, compared with input of 1 km daily ET, with a monthly average error of 0.2% compared with input of 1km month ET. The STARFM model is adaptive to fusing different scales of ET data.

Key words: data fusion, ETWatch, evapotranspiration, TM, MODIS

CLC number: TP72/TP75 **Document code**: A

Citation format: Liu S F, Xiong J and Wu B F. 2011. ETWatch: a method of multi-resolution ET data fusion. *Journal of Remote Sensing,* **15**(2): 255–269

1 INTRODUCTION

Remote sensing image fusion means intelligently integrating different spatial, temporal, and spectral resolution images. Image fusion can complement different information, improve spatial resolution, and provide clarity and synthetic analysis precision (Pohl & Genderen, 1998; Sun & Liu, 1998; Jia, *et al*., 2000). Data fusion deals with the image as a certain rule or an algorithm used to eliminate redundant information, extrude useful and special information, and improve the target identification environment.

Much research has been completed on scale transformation of the land surface parameters. Mayaux & Lambin (1995) established the pixel-based linear relationship between TM data and AVHRR data based on the traditional statistical method. They performed a scale transformation on a vegetation index in two steps. Gao & Alfredo (2002) realized the surface reflectance and LAI scale transformation from ETM data to MODIS data using a Fourier transformation and point-spread function. Kim, *et al*. (2002) researched the downscale transformation of remotely sensed soil moisture with a modified fractal interpolation method. Jin *et al*. (2006) presented surface heterogeneity with the percent of main-land cover class. They implemented the up-scale transformation of the leaf area index (LAI) in the research area by establishing a transformation equation for every land cover class using the correct factor R. Zhang & Zhong (2008) considered the surface heterogeneity in two steps and implemented the upscale transformation of LAI by using ETM data. Many of these scientists researched the scale transformation problem using a data fusion method.

The Moderate Resolution Imaging Spectroradiometer (MODIS) and TM data are commonly used data in remote sensing ET. We can obtain ET data sets in 1 km and 30 m spatial resolutions. The number of MODIS data sets is much more than TM data. For example, in the north of China, we can obtain approximately 80 clear images from MODIS but less than 8 clear images from TM. In order to obtain a high spatial and temporal resolution ET data set, we must fuse the data in different spatial and temporal resolutions from different sensors.

We made use of the high spatial distribution information from high-resolution images and high temporal distribution information from low spatial resolution images so as to present the temporal and spatial distribution with higher precision. Wu & Shao (2006) researched the transformation of different spatial resolution ET data. They used TM data to calculate 30 m resolution ET data and NOAA/AVHRR to calculate 1 km resolution ET data.

Many factors and parameters affect the calculation of ET. It is difficult to perform a data fusion with only input parameters. The non-linear change in data fusion causes much uncertainty in calibrating the parameters and spatial and temporal distribution analysis. Remote sensing ET data fusion needs to integrate the characteristics of input data in spatial distribution and on a temporal scale. In addition, we must evaluate and analyze the fusion result or middle process based on the actual demand.

Received: 2010-03-15; **Accepted**: 2010-08-11

Foundation: The Knowledge Innovation Program of the Chinese Academy of Sciences (No. KZCX1-YW-08-03; No. KZCX1-YW-08-02); The Global Environment Fund Project of World Bank.

First author biography: LIU Shufu (1985—), male, Ph.D candidate, He majors in water resource remote sensing and surface energy balance. E-mail: liushf_263@irsa.ac.cn

Corresponding author: WU Bingfang, E-mail:wubf@irsa.ac.cn

In the paper, we analyzes the spatial characteristics of remote sensing ET in different scales, the data characteristics, and the information before and after fusion. The STARFM model is applied to complete the multi-scale remote sensing ET data fusion in ETWatch.

2 STUDY AREA AND METHODS

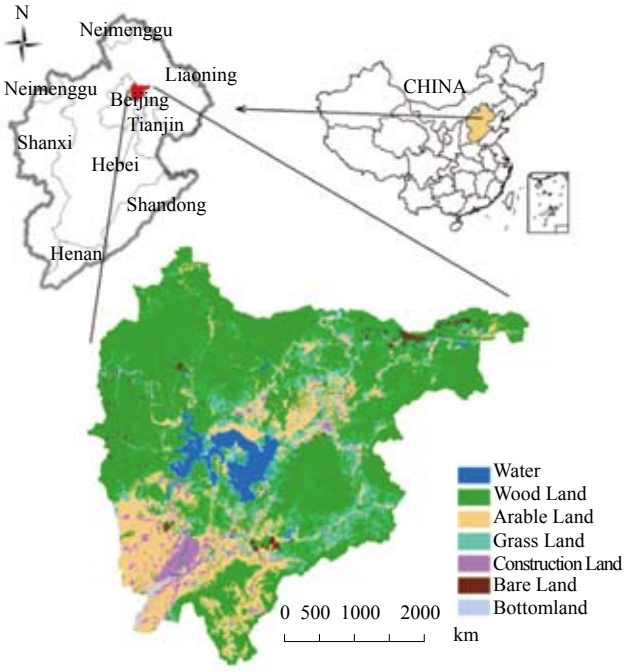

Fig. 1 Location of the research area (Miyun county) and the land use cover

2.1 Study area

In this study, we addressed the area in Miyun County, northeast of Beijing, China. Land-use cover is abundant in this region, such as woodland, arable land, construction land, and water (Fig. 1). A ground station is found in Miyun County,which is located at 116°58′18″E, 40°30′48″N, with an area of 2229.45 km^2. The main land-use type is agriculture, at approximately 1536.89 km^2, which accounts for 69.1% of the total land. Other land use types are construction, approximately 325.68 km^2, accounting for 14.6%; and unused land, at about 363.9 km^2, accounting for 16.3%. The county is surrounded by mountains to the east, north, and west, with the Miyun Reservoir in the middle and the plains to the southwest.

2.2 ET data

We obtained 1 km and 30 m resolution remote sensing ET data from MODIS and TM data. We obtained the MODIS 1B clear-sky data covering the experimental area in May, 2007. We performed the geometric correction using the built-in GCP point of image and calculated the reflectance or radiance, which provided the calibration coefficients. Using threshold values from multiple characteristics, a method that quickly separates clear pixels from cloud-contaminated pixels, we detected cloud pixels (Steve *et al*., 2002). The NDVI in the experimental area was calculated using MODIS 1, 2-band reflectivity after atmospheric correction. Surface albedo was computed with the linear combination of the first seven bands of reflectance. Using MODIS data 31, 32-band radiance, land surface temperature was calculated using the split-window algorithm in the experimental area (Jiang, *et al*., 2006).

We have used a clear TM image from May 28, 2007. The image was pre-processed to determine several parameters, the radiometric calibration, the calculation of surface reflectance, atmospheric correction, calculation of NDVI, and surface temperature inversion (Jose, *et al*., 2004). With the 1∶10,000 topographic map for reference, precision geometric correction was performed with ground control points and with an error rate of less than one pixel.

Low resolution ET data, at 1 km spatial resolution, were generated by the ETWatch system with input parameters from MODIS. These parameters included vegetation index, land surface temperature, surface albedo, surface emissivity, other surface parameters, and meteorological data interpolated by the meteorological station data. We obtained the daily ET data sets for the study by using a gap-filling method generating satellite-free daily ET (Wu, *et al*., 2008; Xiong, *et al*., 2008).

High-resolution ET data, with 30 m spatial resolution, was generated by the ETWatch system with input parameters from the TM data. These parameters included vegetation index, land surface temperature, surface albedo, other surface parameters, and meteorological data from the weather stations (Wu, *et al*., 2008).

Table 1 Dates of images used to calculate ET

Data Type	Data Date		
Low resolution	2007-05-01	2007-05-04	2007-05-06
	2007-05-09	2007-05-14	2007-05-17
	2007-05-25	2007-05-27	2007-05-29
High resolution	2007-05-28	—	—

2.3 Fusion methods

In this paper, we compared several data fusion methods:

(1) Linear transformation

Linear transformation is a simple image fusion method, which directly makes a linear transformation using the corresponding high-resolution ET image pixel with certain requirements (Weng & Tian, 2003). If ET_{tm} is the value of high resolution ET images and Fr is the linear factor generated by the low-resolution ET images, the fused ET images can be obtained by the following equation.

$$ET_{tm}^{f}=ET_{tm}\times Fr \quad (1)$$

Both the concept of linear transformation and the calculation of are simple. However, the temporal information contained in the fused ET images is not enough, and the resulting value is much different from the actual value. The linear factor is determined by the ratio of different periods' low resolution ET data.

(2) Window-based linear transformation

The window-based linear transformation method takes into account the different distributions of the whole image. We set a certain size moving window, and the transformation coefficients were different in each window. The fusion result is defined as:

$$ET_{tm}^{f}(i,j)=ET_{tm}(i,j)\times Fr(i,j) \quad (2)$$

where $ET_{tm}(i, j)$ is the ET value for the high resolution image in the corresponding position (i, j), and $Fr(i, j)$ is the linear factor obtained from low-resolution images in the corresponding window.

The ET temporal and spatial expanding method proposed by Wu in the remote sensing ET temporal and special methods and applications also is based on the window linear transformation method (Wu & Shao, 2006).

(3) Non-linear transformation

The fused ET value does not increase proportionally with the non-linear transformation. The histogram of the fused ET image is close to the low-resolution ET image. The fusion result is defined as:

$$\mathrm{ET}_{\mathrm{tm}}^{\mathrm{f}}(i,j)=\sqrt{\mathrm{ET}_{\mathrm{tm}}(i,j)}\times\sqrt{\max(\mathrm{ET}_{\mathrm{tm}})} \tag{3}$$

where $\mathrm{ET}_{\mathrm{tm}}(i, j)$ is the ET value for the high-resolution image in the corresponding position (i, j), and $\max(\mathrm{ET}_{\mathrm{tm}})$ is the maximum value in the corresponding low-resolution image window.

(4) STARFM Fusion

The basis of the spatial and temporal adaptive reflectance fusion model (STARFM) is that it ignores the errors of spatial location and the atmospheric correction. The value of the low-resolution remote sensing data can be calculated by the high-resolution remote sensing data available for the same period using an area weighted method. The equation is defined as:

$$C_t=\sum\left(F_t^i\times A_t^i\right) \tag{4}$$

where C_t is the pixel value of low-resolution image at time t, i is the spatial index of the high-resolution pixel, F_t^i is the pixel value of the high-resolution image at time t, and A_t^i refers to the area ratio. The algorithm is based on two assumptions: (a) when the low-resolution image pixel value does not change, the high-resolution image pixel value does not change either; and (b) during the predicting period, if the low-resolution image pixel values at time T_1 are equal to the high-resolution image pixel, their values should still be equal.

We first obtained both high and low resolution ET data at the same time (t_1) and then calculated the spatial distribution difference of the images, predicting the high-resolution ET data combined with the low-resolution ET data at another time (t_2). The sliding window method was used to reduce the effect of boundary pixels in the low resolution image. During the calculation, the spatial distance, spectral distance, and time distance were counted as the weights. The prediction ET value for the central pixel based on STARFM can be described with the following equation:

$$\begin{aligned}L(x_{w/2},y_{w/2},T_2)=\sum_{i=1}^{w}\sum_{j=1}^{w}\sum_{k=1}^{n}W_{ijk}\left(M(x_i,y_i,T_2)+\right.\\ \left.L(x_i,y_i,T_1)-M(x_i,y_i,T_1)\right)\end{aligned} \tag{5}$$

where $L(x_{w/2}, y_{w/2}, T_2)$ is the high resolution pixel value at time T_2, w is the size of moving window, only the valid pixel is taken into account in the calculation, $(x_{w/2}, y_{w/2})$ is the middle pixel of a window, $M(x_i, y_i, T_2)$ is the value of the pixel at position (x_i, y_i), $L(x_i, y_i, T_1)$ and $M(x_i, y_i, T_1)$ are corresponding pixel values of high- and low-resolution ET images, respectively, and W_{ijk} is the weight of every pixel in the window. The weight function can be calculated using the following equation.

$$W_{ijk}=1/C_{ijk}\Big/\sum_{i=1}^{w}\sum_{j=1}^{w}\sum_{k=1}^{n}\left(1/C_{ijk}\right) \tag{6}$$

where C_{ijk} is the integrative result of the spectral distance, time, and spatial distance weights that are calculated between the central pixel and other pixels in the window (Gao, *et al*., 2006).

2.4 Evaluation method of the fusion results

Currently, image quality evaluation is divided into subjective evaluation and objective evaluation, and often both are used. Subjective evaluation is analyzed by visual observation, while objective evaluation uses the image information entropy, definition, average gradient, deviation index, root mean square error, and other statistical parameters (Weng & Tian, 2003; Wu, *et al*., 2008). The statistical parameter method is used to evaluate the image quality in the quantitative analysis. The method to evaluate the fusion result of different resolution ET data is different from other multi-source remote sensing data fusion. Using it, the researcher focuses on the problem of whether the fusion result reflects the real value. In this paper, we evaluated the quality of fusion ET data for two aspects: the simulation of phase and the spatial diversity.

(1) The simulation of phase method is used to analyze the accumulation of ET values from fused images and to evaluate whether the fused ET image reflects the accumulation of the fusion phase. Because of the long satellite transit cycle of TM data, it cannot meet the monitoring needs for a long-time series. Through data fusion, the results provide high temporal resolution information.

(2) The spatial diversity method is used to analyze the ET difference of different land cover types before and after fusion. The low-resolution ET data (resolution 1 km) cannot reflect the surface detail characteristics. When integrated with high-resolution ET data, the resulting image possesses high temporal and spatial resolution information.

3 FUSION RESULTS

Linear transformation integrates the high- and low-resolution ET data by way of linear stretch. Non-linear transformation changes the ET value in different proportions based on the data range of the ET data. The STARFM method takes into account the spatial, spectral, and time distance of high- and low-resolution ET data. We compared the fusion results of these three methods—linear transformation, non-linear transformation, and the STARFM method. Then we analyzed the results from the STARFM method in the simulation of phase and the spatial diversity.

3.1 Fusion method comparison using daily ET data

In order to compare the differences in the four fusion methods, we used the TM data from May 28, 2007, to calculate the ET and then fused the high spatial resolution ET data from May 28th using the four fusion methods separately. We compared the results with the input of high-resolution and low-resolution ET data (Fig. 2).

The linear transformation stretches the high-resolution ET data over the entire image and well preserves the spatial distribution information of high resolution, but it cannot present the characteristics of the low-resolution ET data. The value ranges and average value of window-based linear transformation and the statistics are the same as the linear transformation. However, the stretch in each value range is not the same as that of the window-based linear transformation. This is relative to the different transform coefficient in each window. The non-linear transformation expands the range of the value in the fusion results. In the non-linear transformation, the low values increased more, and the average value of the whole

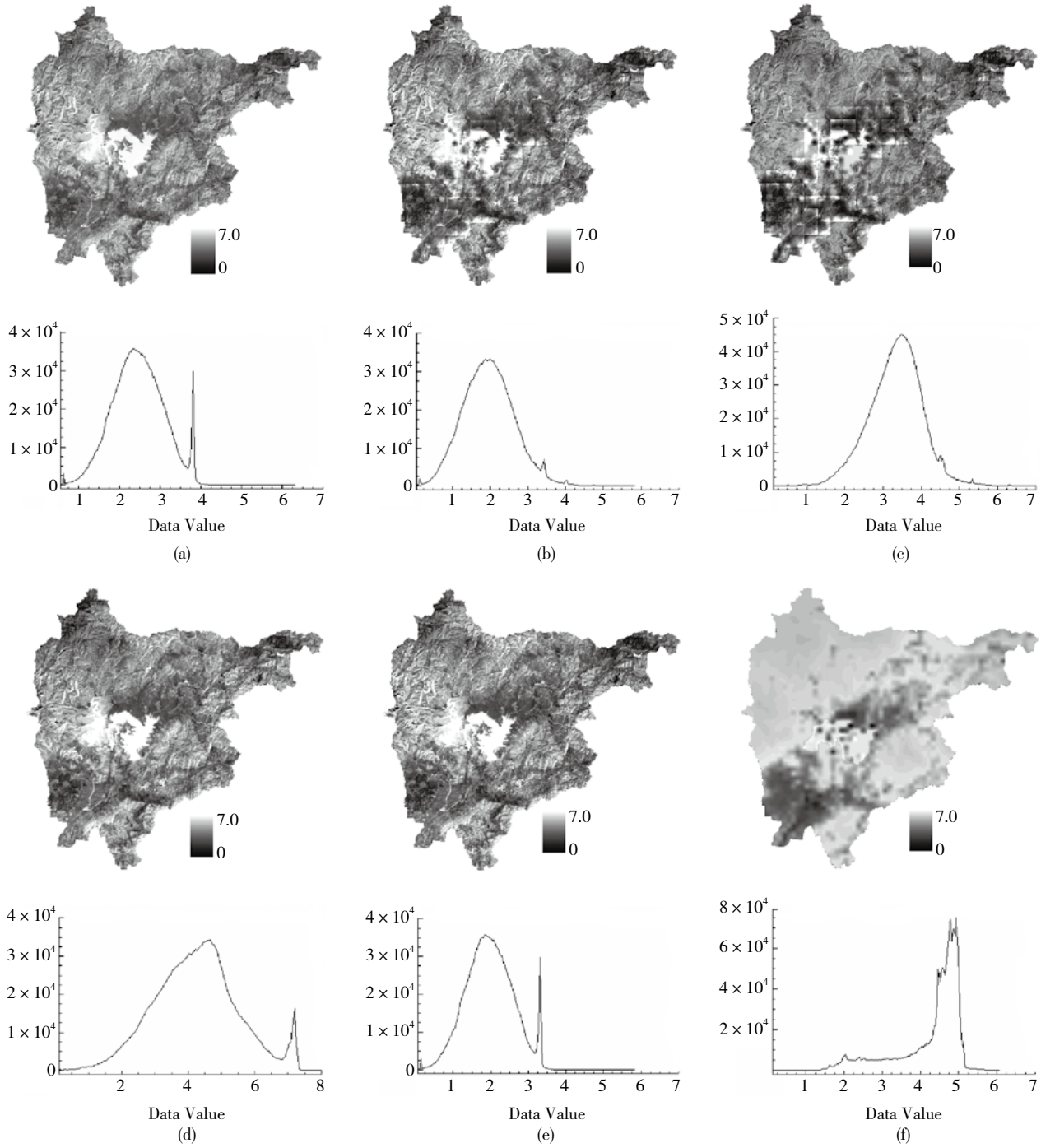

Fig. 2 Comparison of different fusion method results with input ET data
(a) Linear transformation; (b) Window-based linear transformation; (c) Non-linear transformation;
(d) STARFM fusion model; (e) Input 30 m ET Data; (f) Input 1 km ET Data

Table 2 The statistics of different fusion methods

Fusion methods/Statistics	Minimum /mm	Maximum /mm	Average /mm	STDV	Avg/30 m/%	Avg/1 km/%
Linear	0.55	6.32	2.49	0.63	20.48	– 284.13
Window-based	0.05	5.82	1.98	0.68	0.00	– 338.24
Non-linear	0.12	7.39	3.35	0.7	40.90	– 132.86
STARFM	0.11	7.47	4.26	1.14	53.52	– 1.75
30 m Original ET	0.05	5.82	1.98	0.63	0.00	—
1 km Original ET	0.12	6.06	4.28	0.86	—	0.00

* Avg/30 m means the Average value compares with the 30m original ET; Avg/1 km means the Average value compares with the 1 km original ET

image was about 3.35 mm (Table 2).

The value range of the results based on the STARFM method in ETWatch and the image's average value are consistent with the 1km resolution data. The histogram of the resulting image is distributed equally and is similar to the 30 m resolution data. The results of the STARFM method reflect the character of high-resolution data in spatial distribution and also import the characteristics of low-resolution data. The difference between fusion results and input 1 km ET data were 284.13%, 338.24%, 132.86% and 1.75%, respectively, for the different methods—linear transform, window-based linear transform, non-linear transform, and STARFM fusion model.

3.2 Analysis of Monthly ET Data Fusion Results

We compared 1 km resolution monthly ET data before fusion with the monthly ET data after fusion, which was calculated using the STARFM model in ETWatch (Fig. 3).

Table 3 Statistical comparison of monthly fusion results and 1 km monthly ET input

	Minimum	Maximum	Average	St Dev
STARFM	4.42	145.48	85.92	27.51
1 kmET	1.51	137.41	86.13	23.67
Difference/%	192.7	5.9	– 0.2	16.2

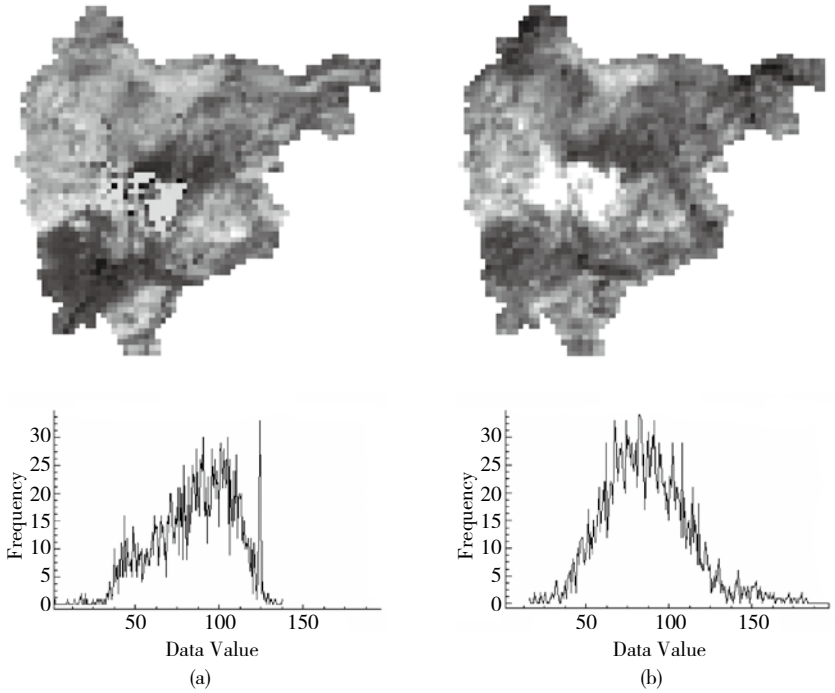

Fig. 3 Miyun ET distribution map in May 2007
(a)1 km monthly ET; (b) fusion result

The range of fused images is consistent with the 1 km resolution data, which is related to the high-temporal resolution of 1 km ET images. The ET value of the image is within the range of 40mm to 140 mm. The average of the image is basically the same as the input 1 km ET data, the difference is 0.2%, and the standard deviation difference is 16.2% (Table 3, Fig. 3). The histogram of the fused image combines features of 1 km data and 30 m data. The trend of the histogram is consistent with the 1 km ET data, which shows that the results preserve the temporal character of low-resolution ET data.

In the 1 km resolution scale, the results are consistent with the 1km input ET data, the result is well-correlated with the input data, and the coefficient is 0.9, as shown in Fig. 4. The image after fusion integrates the characteristics of both high & low resolution data.

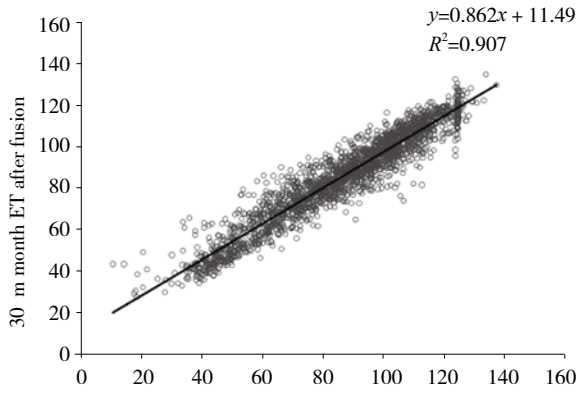

Fig. 4 The scatter of ET data before and after fusion

3.3 Fusion result analysis of representative land cover types

The spatial diversity reflects the ET spatial differences between different land cover types. Whether the results reflect the diversity of different land cover types directly reflects the quality of fusion data.

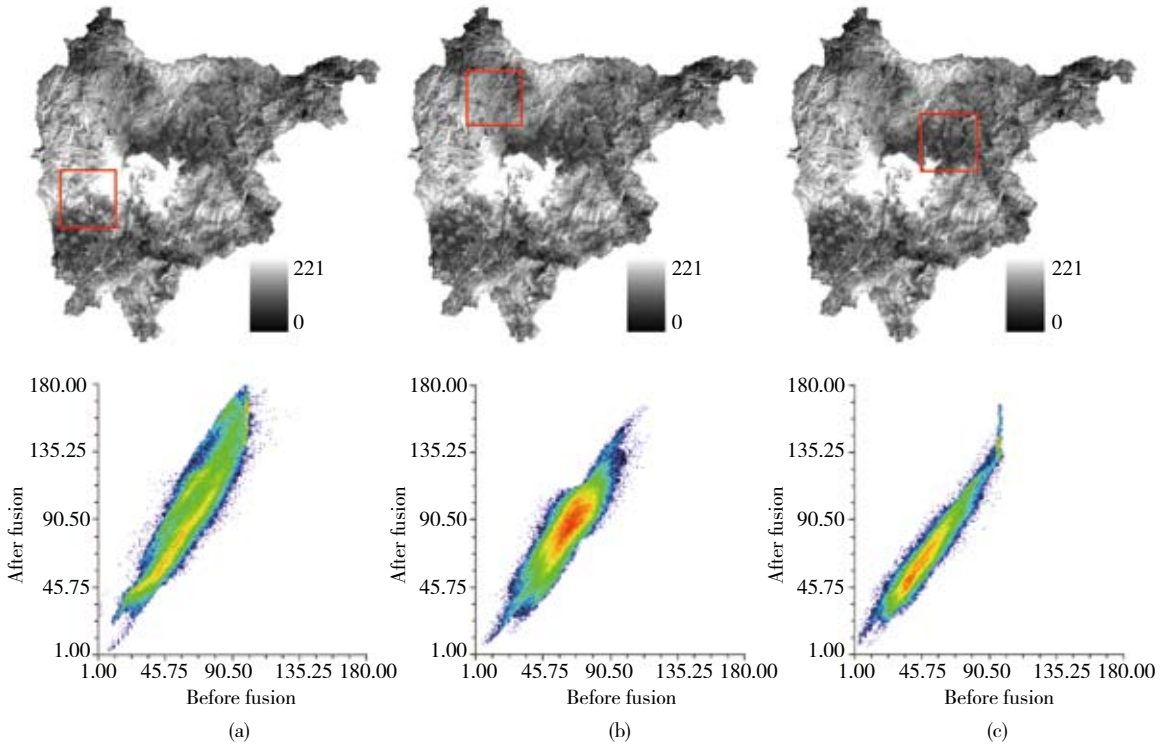

Fig. 5 ET distribution scatter plots of different land use types
(a) Arable land and water; (b) Wood land and bare ground; (c) Water, arable land and wood land

We compared the fusion image with the single-day ET calculated using TM data, and the results show that the diversity characteristics of ET values after fusion are consistent with the data before fusion. The fused image retained the diverse characteristics of the original TM image. We analyzed the fusion results with different land-use types (Fig. 5). The land-use types of the two-dimensional plot in the Fig. 5(a) are mainly arable land and water. The land-use types of the two-dimensional plot in the Fig. 5(b) are mainly woodland, bare ground, and arable land. The land-use types of the two-dimensional plot in the Fig. 5(c) are mainly water, arable land, and woodland. The horizontal axis of the scatter plot represents ET values of images before fusion, and the vertical axis represents the fused images. We changed the single-day ET to monthly ET with a linear transformation before plotting the scatter. The linear transformation preserves the spatial distribution of the original ET data.

We can see the ET distribution before and after the data fusion from the two-dimensional scatter plot. The differences in ET values are apparent among the different land-use types. The distribution of water, woodland, arable land, and bare ground show good correlation both before and after fusion. This means that the fused image retained the original spatial distribution information and can reflect the ET difference of different land-use types. A tail is seen in the right scatter plot, which represents the water in the land-use type. The monthly ET image before fusion is transformed from a single-day ET image, and the monthly ET value of water before fusion is about 100 mm. The fused ET image reflects the changing information of low-resolution data over a month, and the water ET value is approximately 135 mm to 150 mm. Therefore, a tail-like distribution area appears in the scatter plot. This also shows the diversity of the ET values for different land-use types after fusion.

4 DISCUSSION AND CONCLUSION

The STARFM fusion method combines temporal changing information from MODIS with spatial distribution information from TM and generates ET data sets with high spatial and temporal resolution data. The data sets retain the temporal trend of high temporal resolution data and reflect the spatial detail differences of high spatial resolution data. The relative error of daily ET between STARFM and input 1 km daily ET is 1.75%, and the monthly ET relative error is 0.2%. The STARFM model can improve remote monitoring spatial and temporal precision.

The fusion results are different among different land-use types. The error in arable land is smaller than for woodland and city because of the small land cover change difference and the plains land.

The STARFM is still a weighted transformation fusion method. The result is related to the complexity of the underlying surface types. If small crops are on the land, such as crops and water at the junction, the fused ET value is not very good because of different weights produced by different land features. Therefore, we need to develop a method to process the boundary phenomenon.

The temporal distribution of high-resolution data may affect the fusion results. If the dates of the high & low resolution data are far from each other, the change in surface character, especially the vegetation cover, and weather condition changes that are related to the ET, can affect the fusion results. In this situation, the fusion method may not display this change information. If the temporal difference between the result date (t_2) and the input data date (t_1) is small, the result will well-reflect the spatial distribution character of the high-resolution data. The error in the fusion result is more apparent if the temporal difference between t_2 and t_1 is great because of the change

in surface characteristics. Therefore, we need to use more high-resolution data in the fusion process.

At present, the 30 m resolution images that we are able to obtain include TM, ETM, BJ-1, CBERS, and HJ-1, among others. All these images come from different sensors and have their own characteristics. An important step is to normalize and correct high-resolution images from different sensors, which is important for the next step in determining the different spatial and temporal resolution fusion methods.

With the increase in multi-source remote sensing images, the demand for data fusion is also increasing. The future trend will be integration of multi-source remote sensing data. The research in the field of multi-source remote sensing data fusion will be to determine the conditions and the methods before doing the fusion, based on the characteristics of the model and the problem.

The linear transformation method retains the spatial distribution information of the high-resolution data but cannot reflect the temporal changing information. The non-linear transformation method enhances the temporal changing information.

The STARFM method synthetically takes into account the spatial, spectral, and temporal information, and the results integrate the characteristics of both high and low resolution data. The method is adaptive to fusing different scales of remote sensing ET data.

REFERENCES

Gao F, Masek J, Schwaller M and Hall H. 2006. On the blending of the Landsat and MODIS surface reflectance: Predicting daily Landsat surface reflectance. *IEEE Transactions on Geosciences and Remote Sensing*, **44**(8): 2207–2218

Gao X and Huete A R. 2002. Validation of MODIS land surface reflectance and vegetation indices with multi-scale high spatial resolution data. *Geosciences and Remote Sensing Symposium*, **2**: 533–535

Jia Y H, Li D R and Sun J B. 2000. Data Fusion Techniques for Multi-sources Remotely sensed Imagery. *Remote sensing technology and application*, **15**(1): 41–44

Jiang L P, Qin Z H and Xie W. 2006. Program splits window algorithm to retrieve land surface temperature for MODIS data using IDL. *Geomatics & Spatial Information Technology*, **29**(3): 114–117

Jin Z, Tian Q, Chen J M and Chen M. 2006. Spatial Scaling Between Leaf Area Index Maps of Different Resolutions. *Journal of Environmental Management*, **85**(3): 628–637

Jose A S, Juan C J and Leonardo P. 2004. Land surface temperature retrieval from LANDSAT TM5. *Remote Sensing of Environment*, **90**(4): 434–440

Kim G and Barros A P. 2002. Downscaling of remotely sensed soil moisture with a modified fractal interpolation method using contraction mapping and ancillary data. *Remote Sensing of Environment*, **83**(3): 400–413

Mayaux P and Lambin E T. 1995. Estimation of tropical forest area from coarse spatial resolution data: a two-step correction function for proportional errors due to spatial aggregation. *Remote Sensing of Environment*, **53**(1): 1–15

Pohl C and Genderen J L. 1998. Multi-sensor image fusion in remote sensing: concepts, methods and applications. *International Journal of Remote Sensing*, **19**(5): 823–854

Steve Ackerman, Kathleen Strabala, Paul Menzel, Richard Frey, Chris Moeller, Liam Gumley, Bryan Baum, Suzanne Wetzel Seeman, and Hong Zhang. 2002. Discriminating Clear-Sky from Cloud with MODIS Algorithm Theoretical Basis Document (Mod35), Version 4.0

Sun J B, Liu J L and Li J. 1998. Multi-source remote sensing image data fusion. *Journal of remote sensing*, **2**(1): 47–50

Weng Y L and Tian Q J. 2003. Analysis and Evaluation of method on remote sensing data fusion. *Remote Sensing Information*, **37**(3): 49–53

Wu B F, Xiong J, Yan N N, Yang L D and Du X. 2008. ETWatch: Methodology of regional evapotransp iration monitoring with remote sensing. *Advances in Water Science*, **19**(5): 671–678

Wu B F and Shao J H. 2006. Temporal and spatial extension of evapotranspiration estimated from remote sensing. *Journal of Hydraulic Engineering*, **37**(3): 286–292

Wu J , Jiang H and Li Y H. 2008. Quality Assessment of RS image fusion. *Geomatics Technology and Equipment*, **10**(4): 9–11

Xiong J, Wu B F, Yan N N, Hu M G and Sun X M. 2008. Research on Temporal Reconstruction of Evapotranspiration by Using Remote Sensing. *Progress in Geography*, **27**(2): 53–59

Zhang W C, Zhong S and Hu S Y. 2008. Spatial scale transferring study on Leaf Area Index derived from remotely sensed data in the Heihe River Basin, *Chian*. *Acta Ecologica Sinica*, **28**(6): 2495–2502

ETWatch中不同尺度蒸散融合方法

柳树福，熊隽，吴炳方

中国科学院 遥感应用研究所，北京 100101

摘 要：高分辨率遥感蒸散数据集的构建受到数据源的限制和云的影响，单一传感器无法达到高时空分辨率覆盖。本文分析了ETWatch不同尺度遥感蒸散结果的空间特征，通过几种融合方法的比较，分析数据融合前后的数据特征和信息量，将时空适应性反射率融合模型（STARFM）集成到ETWatch，用于不同尺度遥感蒸散数据的融合，该方法可以很好的结合高低分辨率数据的空间分布和时间分布信息，在时间上保留了高时间分辨率数据的时间变化趋势，空间上又反映了高空间分辨率数据的空间细节差异，STARFM融合后的日ET数据与融合前1 km 日ET数据的平均相对误差为1.75%，融合后的月ET数据与融合前1 km 月ET数据的平均相对误差为0.2%，STARFM适合于不同尺度下遥感ET数据的融合。

关键词：图像融合，ETWatch，蒸散发，TM，MODIS

中图分类号：TP72/TP75 **文献标志码**：A

引用格式：柳树福，熊隽，吴炳方. 2011. ETWatch中不同尺度蒸散融合方法. 遥感学报，**15**(2): 256–269
Liu S F, Xiong J and Wu B F. 2011. ETWatch: a method of multi-resolution ET data fusion. *Journal of Remote Sensing*, **15**(2): 255–269

1 引 言

遥感影像融合指将具有不同空间分辨率、时间分辨率和光谱分辨率的影像数据智能化合成，实现多种信息资源的相互补充，改善遥感影像的空间分辨率和清晰度，提高遥感影像的综合分析精度（Pohl 和Genderen，1998；孙家柄和刘继林，1998；贾永红 等，2000）。数据融合不是不同数据间的简单复合迭加，而是按照一定的规则或算法进行运算处理，消除冗余或互补信息，突出有用专题信息，改善目标识别的图像环境。

国内外学者对不同的地表参数的尺度转换问题开展了相关研究。Mayaux 和 Lambin （1995）在传统统计方法的基础上，建立了TM数据与AVHRR数据之间基于像元的线性关系，运用两步式的转换方法进行了植被指数的尺度转换。Gao 和 Huete （2002）用傅里叶变换和传感器的点扩散函数，实现从ETM向MODIS的地表反射率及LAI的尺度转换。Kim 和 Barros （2002）研究了用可变不规则碎片插值方法进行遥感土壤湿度的向下尺度转换。Jin等（2006）用主导覆盖类面积百分比来表征地表异质性，通过校正因子R建立各覆盖类尺度转换公式，实现了研究区LAI升尺度转换。张万昌等（2008）利用ETM数据，分两步考虑了地表异质性，实现了LAI升尺度转换。

MODIS和TM是遥感蒸散估算中常用的数据，获取的蒸散产品分别为1 km和30 m空间分辨率，而MODIS的有效时相数据比TM更丰富。以华北地区为例，每年可获取晴空可见光和热红外数据约80景，TM则不到8景，获取高时空分辨率蒸散数据集的解决方法之一就是将不同传感器上具有不同时空分辨率特征的数据进行融合，充分利用高分辨率遥感影像提供的蒸散量空间分布信息和低分辨率遥感影像提供的蒸散量时间变化信息，从而在更精细的时间空间尺度上反映蒸散量的时空变化。吴炳方等（2006）用TM影像计算的30 m分辨率蒸散与用NOAA/AVHRR计算的1 km分辨率ET相结合，作了蒸散量数据的不同空间分辨率的转换研究。

收稿日期：2010-03-15；**修订日期**：2010-08-11

基金项目：中国科学院知识创新工程重大项目（编号：KZCX1-YW-08-03；编号：KZCX1-YW-08-02）；世界银行GEF项目。

第一作者简介：柳树福（1985— ），男，湖南浏阳人，中国科学院遥感应用研究所博士研究生，目前主要从事水资源遥感及地表能量平衡研究。E-mail:liushf_263@irsa.ac.cn。

通信作者：吴炳方，E-mail:wubf@irsa.ac.cn。

由于蒸散计算中的因子众多，在输入参量层次上进行数据融合尤为困难，数据融合中发生的非线性变化给参量的标定、参量的时空特征分析也带来了较大的不确定性。遥感蒸散数据的融合要在空间分布和时间尺度上综合原数据的特征，蒸散数据融合的目的要求按照实际需求去评价和分析融合的结果或中间过程。

本文分析了不同尺度遥感蒸散结果的空间特征，分析数据融合前后的数据特征和信息量，在ETWatch利用STARFM方法实现了多尺度遥感蒸散结果融合。

2 数据与方法

2.1 研究区

本研究选择位于北京市东北部密云地区作为实验区，实验区有林地、耕地、建筑用地和水体等多种土地利用类型，地表覆盖类型和景观结构丰富，并且在密云新城子镇设有地面观测站。实验区的中心坐标为116° 58′18″E，40° 30′48″N，面积为2229.45 km^2，范围内主要的土地利用类型为农业用地1536.89 km^2，占69.1%，其中耕地占14.2%，园地占12.6%，林地占71.5%；建设用地325.68 km^2，占14.6%；未利用地363.9 km^2，占16.3%，其中荒草地占92.6%，沙地、裸土等占7.4%。全县东、北、西三面群山环绕，中部是密云水库，西南是洪积冲积平原，总地形为三面环山，中部低缓，西南开口的簸箕形（图1）。

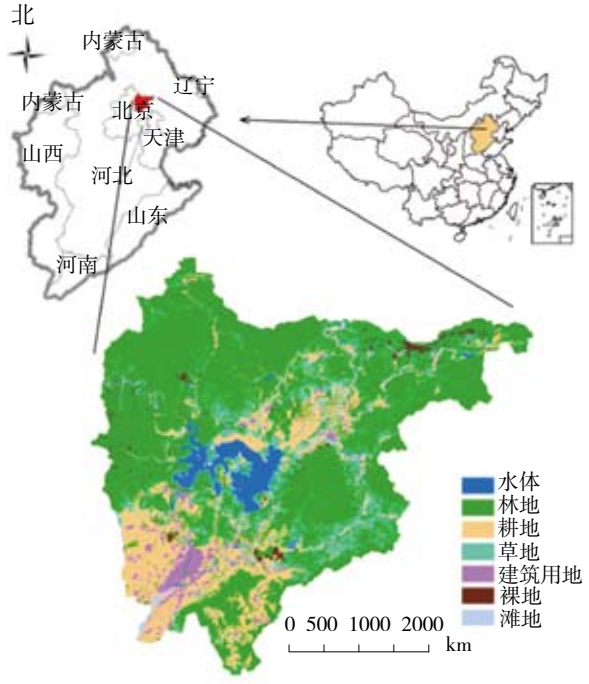

图1 研究区位置及土地利用图

2.2 蒸散数据

1 km和30 m的遥感蒸散量数据分别利用MODIS数据和TM数据采用ETWatch估算得到（数据日期见表1）。获取了实验区2007年5月无云污染的MODIS 1级产品数据，采用MODIS数据内置的GCP点完成图像的几何纠正，并根据提供的定标系数将数据定标为所需的反射率或辐亮度。通过多个特征进行阈值判定，快速实现陆地上空晴空像元与云污染像元的分离，进行云检测（Steve Ackerman，2002）。用大气校正后的1、2波段反射率，计算得出实验区1 km分辨率NDVI。用MODIS数据的前7个波段的反射率的线性组合计算地表反照率。采用MODIS数据的31、32波段的辐亮度，通过分裂窗算法计算得出实验区1 km分辨率地表温度（姜立鹏 等，2006）。

研究使用2007年5月无云污染的1景TM数据（2007-05-28）。对影像数据进行了辐射定标、地表反射率的计算、大气纠正及NDVI的计算，以及地表温度的反演（Jose 等，2004）。以1∶10万地形图为参照，通过输入地面控制点对影像进行几何精纠正，误差控制在1个像元以内。

低分辨率ET数据是用MODIS数据生成植被指数、地表温度、地表反照率和地表比辐射率等地表参数，以及气象观测站的通过插值的气象数据，通过ETWatch系统生成的空间分辨率为1 km的ET分布数据。并利用时间拓展生成无卫星过境日的ET，得到实验区的逐日ET数据集（吴炳方 等，2008；熊隽等，2008）。

高分辨率ET数据是用TM数据生成植被指数、地表温度、地表反照率等地表参数，以及气象观测站的气象数据通过ETWatch系统生成的空间分辨率为30 m的ET分布数据（吴炳方 等，2008）。

表1 所使用的高分辨率和低分辨率蒸散量结果日期

数据类型	数据日期		
低分辨率	2007-05-01	2007-05-04	2007-05-06
	2007-05-09	2007-05-14	2007-05-17
	2007-05-25	2007-05-27	2007-05-29
高分辨率	2007-05-28	—	—

2.3 融合方法

线性变换是把高分辨的ET数据按线性的方式进行融合，基于窗口的线性变换是在每个窗口中按照不同的变换因子进行变换，非线性变换是对不同范围的

ET数据按不同的比例进行变换，基于STARFM方法考虑了高低分辨率ET数据的空间距离、光谱距离及时间距离，从而进行融合。

（1）线性变换：线性变换是一种简单的影像融合方法，它直接将高分辨率ET影像对应像素点的值按照一定要求作线性变换（翁永玲和田庆久，2003）。如果ET_{tm}为高分辨率影像的ET值，Fr为由低分辨率影像生成的线性因子，那么融合后影像ET_{tm}^{f}可通过下式得到：

$$ET_{tm}^{f}=ET_{tm}\times Fr \tag{1}$$

线性变换的优点在于概念简单，计算量非常小。缺点是融合后的图像包含的时间信息不强，融合结果与实际值相差太大，线性变换因子的确定由不同时间段低分辨率ET的比值确定。

（2）基于窗口的线性变换：基于窗口的线性变换方法考虑到整幅影像的差异，设置固定尺寸的移动窗口，每个窗口的变换系数各不相同，融合结果ET_{tm}^{f}为：

$$ET_{tm}^{f}(i,j)=ET_{tm}(i,j)\times Fr(i,j) \tag{2}$$

式中，$ET_{tm}(i,j)$为高分辨率影像在对应位置(i,j)的ET值，$Fr(i,j)$为通过低分辨率影像在对应区域得到的线性因子。吴炳方等人（2006）在遥感估算蒸腾蒸发量的时空尺度推演方法及应用中提出的ET时空尺度推演方法也是基于窗口的线性变换方法。

（3）非线性变换：非线性变换使ET值不按比例增长，通过变换后使高分辨率图像的直方图与低分辨率图像接近，融合后影像$ET_{tm}^{f}(i,j)$可表示为：

$$ET_{tm}^{f}(i,j)=\sqrt{ET_{tm}(i,j)}\times\sqrt{\max(ET_{tm})} \tag{3}$$

式中，$ET_{tm}(i,j)$为高分辨率影像在对应位置(i,j)的ET值，$\max(ET_{tm})$是对应窗口区域低分辨率图像的最大值。

（4）STARFM融合方法：STARFM方法的理论基础是在忽略空间定位误差与大气纠正误差的前提下，低分辨率遥感数据的像元值可以用同期高分辨率遥感数据像元值的面积比例的加权平均来计算，如式（4）所示：

$$C_t=\sum\left(F_t^i\times A_t^i\right) \tag{4}$$

式中，C_t是t时间低分辨率遥感数据的像元值，i为低分辨率遥感数据像元所对应高分辨率遥感数据像元的索引号，F_t^i为t时间的高分辨率遥感数据像元值，A_t^i为其面积比例。算法有两个假定：当低分辨率影像的像元值没有发生变化时，高分辨率影像的像元值也不发生变化；在预测时间窗口内，如果T_1时间的低分辨率影像像元值与高分辨率影像的像元值相等，那么在T_2时间它们的值仍然相等。

STARFM方法首先获取同一时间（t_1）的高分辨率ET与低分辨率ET，通过计算影像间空间分布的差异，结合另一时间（t_2）的低分辨率ET数据进行相应时间高分辨率ET的预测。在预测过程中使用了滑动窗口的方法来减少低分辨率遥感数据像元边界的影响，在使用滑动窗口进行中心像元值的计算时，把空间距离、光谱距离及时间距离作为权重。基于STARFM的预测算法可以用式（5）进行描述：

$$L(x_{w/2},y_{w/2},T_2)=\sum_{i=1}^{w}\sum_{j=1}^{w}\sum_{k=1}^{n}W_{ijk}\left(M(x_i,y_i,T_2)+L(x_i,y_i,T_1)-M(x_i,y_i,T_1)\right) \tag{5}$$

式中，L（$x_{w/2}$，$y_{w/2}$，T_2）是预测的T_2时刻的高分辨像元值，w是移动窗口的大小，窗口中只使用有效像元用来进行预测，$(x_{w/2}, y_{w/2})$是窗口中间的像元，$M(x_i, y_i, T_2)$是窗口位置(x_i, y_i)处在T_2时刻的像元值，$L(x_i, y_i, T_1)$和$M(x_i, y_i, T_1)$则是高分辨率ET和低分辨率ET在T_1时刻的相应像元值，W_{ijk}为窗口内各像元在预测中心像元时的权重。STARFM算法中的权重函数可以用式（6）进行计算：

$$W_{ijk}=1/C_{ijk}\Big/\sum_{i=1}^{w}\sum_{j=1}^{w}\sum_{k=1}^{n}\left(1/C_{ijk}\right) \tag{6}$$

式中，C_{ijk}是由窗口中心的预测像元与窗口中其他像元（包括多时相数据）的光谱距离、时间距离与空间距离计算的产品（Gao 等，2006）。

2.4 融合结果的评价方法

目前对影像质量评价分为主观评价和客观评价，并相结合使用。主观评价是通过目视观察进行分析，客观评价是利用图像的信息熵、清晰度、平均梯度、偏差指数和均方根误差等统计参数进行判定（翁永玲和田庆久，2003；武坚 等，2008）。统计参数的评价方法是从定量的角度评价图像的质量，不同分辨率ET数据融合结果的评价与其他多源遥感数据融合的评价方法不一样，更侧重于对ET融合结果是否反映真实情况来考虑。本文从时相模拟性和地物分异性两个方面评价ET数据融合结果的质量。

（1）时相模拟性分析，从融合后的ET数据是否反映了融合时段过程中ET量的积累来分析融合结果

的时相模拟性。由于TM数据卫星过境周期长，高分辨率ET数据的时间分辨率太低，不能满足长时间序列ET监测的需求。通过数据融合，使融合后的ET数据具有高时间分辨率信息。

（2）地物分异性分析，从融合后的ET数据是否反映了不同地物下的ET差异来分析融合结果的地物分异性。低分辨率ET数据（分辨率1 km）不能反映地表的详细特征，通过与高分辨率ET数据的融合，生成具有高时空分辨率的ET数据。

3 融合结果

对线性变换、非线性变换和ETWatch系统中的STARFM方法的融合结果作了比较，并在比较的基础上，选择STARFM融合方法，进一步从时相模拟性和空间分异性两方面分析融合前后影像的特征。

3.1 单日ET数据的融合方法比较

为了比较这几种融合方法的差异，选用2007-05-

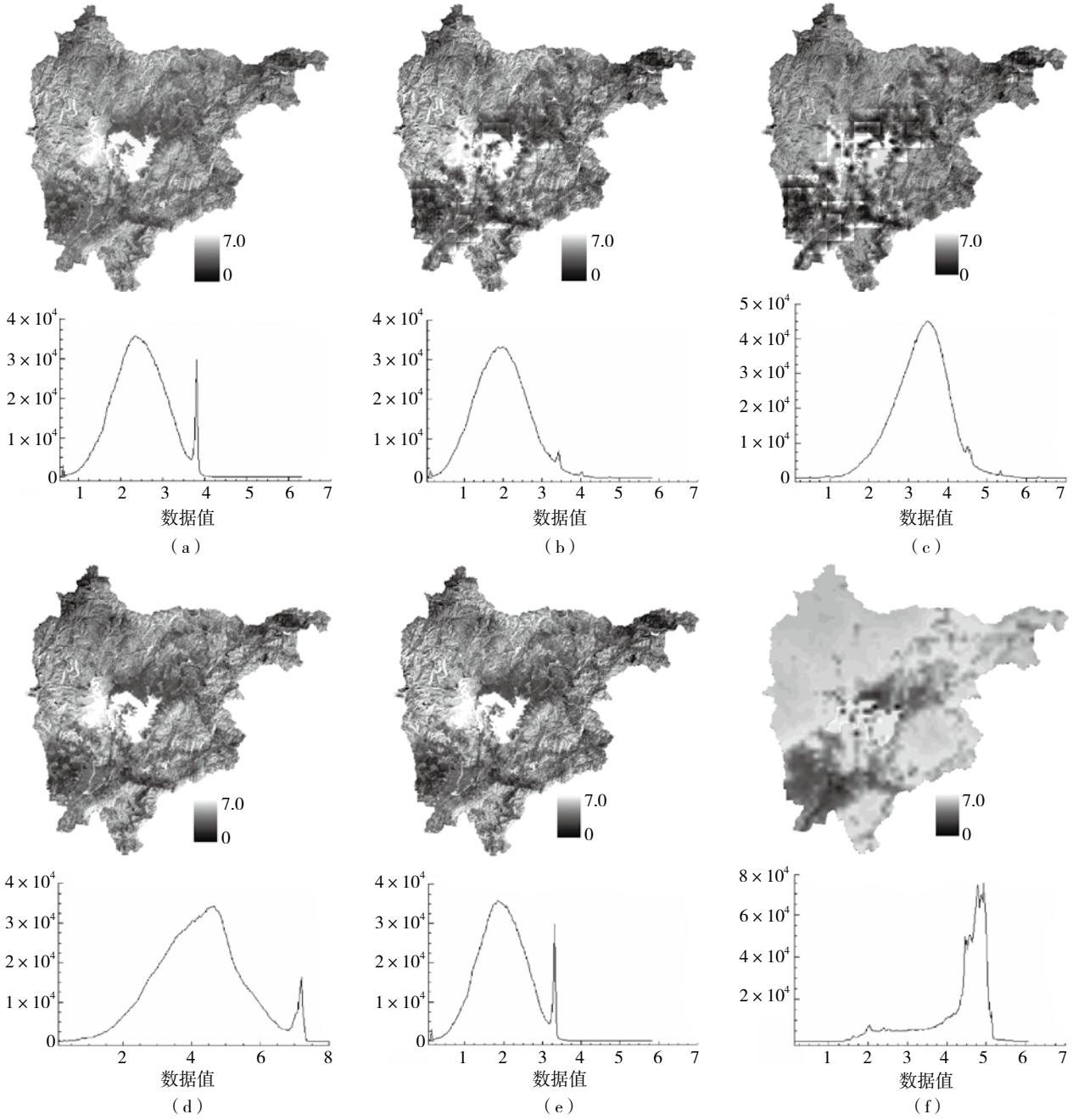

图2 不同融合方法结果和原始ET数据对比

（a）线性变换结果；（b）基于窗口的线性变换结果；（c）非线性变换结果；（d）STARFM融合结果；（e）30 m融合前ET数据；（f）1 km融合前ET数据

28一景TM通过ETWatch系统计算的ET数据，利用这一天的高分辨率ET数据与低分辨率ET数据按照以上4种方法分别融合出2007-05-28的高分辨ET数据，并与输入的高分辨率和低分辨率ET数据进行对比分析。得到的结果如图2：

从图2中的直方图以及融合结果的统计特征（表2）可以看出，线性变换在整体上对高分辨率ET数据做了拉伸，可以很好地保留了高分辨率ET数据的空间分布信息，但是不能体现出低分辨率ET数据的数据特征。基于窗口的线性变换的融合结果的值域范围与高分辨率ET基于一致，其平均值也一致，统计量与高分辨率ET相似。但经过变换后空间分布特征发生了较大的变化，基于窗口的线性变换在每个值域区间的拉伸不一致，这是与每个窗口的线性变换系数不一致相关。非线性变换扩大了融合结果的值域范围，通过非线性变换，低值部分增加得多，高值部分增加得相对少，整幅影像的平均值大概为3.35 mm（见表2）。

ETWatch系统中STARFM方法的融合结果的值域范围与1 km的ET数据基本保持一致，图像的均值与1 km的ET相一致；直方图分布均匀，与30 m的ET数据的直方图形状相似，因值域的拉伸，图像的标准差比30 m的ET数据增加，为1.14。STARFM融合结果在空间分布上很好的反映了高分辨率ET数据的特征，同时也引入了低分辨ET数据的数据特征。线性变换、基于窗口的线性变换、非线性变换和STARFM融合的验证点与1 km融合前ET数据的差异分别为284.13%、338.24%、132.86%和1.75%。基于STARFM的融合方法的结果与1 km融合前ET数据一致性最好。

3.2 月ET数据的融合效果

将计算的1 km融合前月ET数据和ETWatch系统中STARFM融合后的2007年5月ET数据（重采样到1 km）进行对比分析（图3）。

表2 不同融合方法结果的统计特征

融合方法/统计量	最小值/mm	最大值/mm	平均值/mm	标准方差	均值与原30 m ET比较/(%)	均值与原1 km ET比较/(%)
线性变换	0.55	6.32	2.49	0.63	20.48	–284.13
基于窗口的线性变换	0.05	5.82	1.98	0.68	0.00	–338.24
非线性变换	0.12	7.39	3.35	0.7	40.90	–132.86
STARFM融合	0.11	7.47	4.26	1.14	53.52	–1.75
30 m融合前ET	0.05	5.82	1.98	0.63	0.00	—
1 km融合前ET	0.12	6.06	4.28	0.86	—	0.00

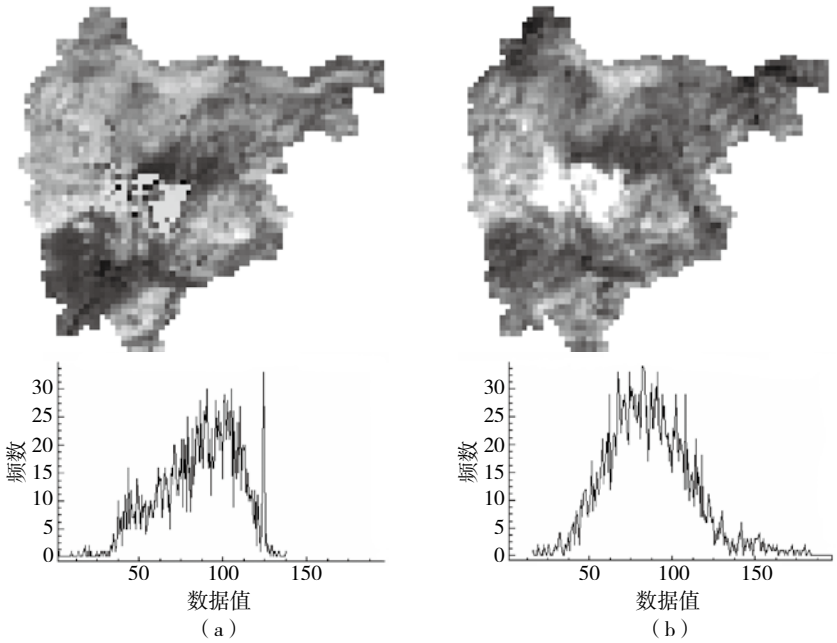

图3 密云2007年5月ET分布图

（a）1 km月ET；（b）融合结果

表3 月融合结果与1 km月ET数据统计特征对比

	最小值	最大值	平均值	标准差
STARFM	4.42	145.48	85.92	27.51
1 km ET	1.51	137.41	86.13	23.67
差异／%	192.7	5.9	–0.2	16.2

融合后的影像的值域与1 km分辨的数据基本一致，融合后影像的数值主要分布在4—140 mm区间，并且区域的ET平均值与输入的1 kmET数据一致，差异为0.2%，标准方差差异为16.2%（表3、图3）。STARFM融合影像结合了1 km数据和30 m数据的特征，融合后影像的直方图与1 km蒸散数据的直方图基本一致，这反映了STARFM融合结果保留了低分辨率数据的时相特征。

在1 km尺度上，融合后的ET数据与1 km分辨ET数据相一致，具有很好的相关性，相关系数为0.9，见图4。融合后的ET数据很好得保持了高低分辨率两种数据的特征。

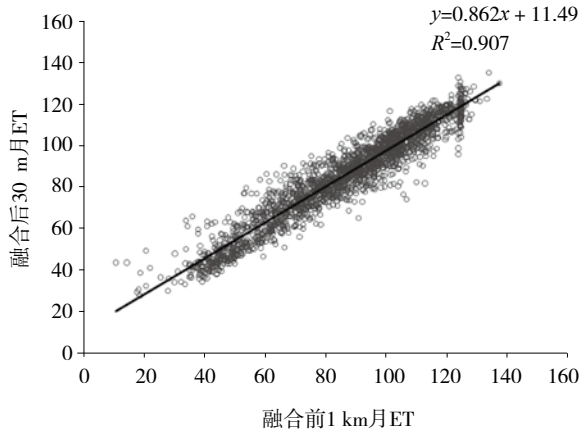

图4 1 km尺度上融合前后数据比较

3.3 典型地物融合效果分析

地物分异性是影像上反映的不同地物类型的ET空间分布差异。融合结果是否反映了不同地物类型差异直接体现了融合结果的质量。

将融合后的月ET结果与利用TM数据计算的单天的ET数据进行比较分析，发现融合前后ET数据的地物分异特征在整体上基本一致。融合后的影像基本保持了原TM影像的地物差异特征（图5）。图5（a）方框的二维散点图中显示的土地利用类型主要是耕地和水体；图5（b）方框二维散点图中显示的土地利用类型主要是林地、裸地和耕地；图5（c）方框的二维散点图中显示的土地利用类型主要是水体、耕地和林地。由于融合前的影像是单天的ET值，在与融合后的月的ET数据进行散点图比较时先线性变换到月的ET值，这样可以保持影像的空间分布性不变。

在二维散点图上可以看出融合前后影像的分布特征，不同地物类型ET分异明显，水体、林地、耕地和裸地的分布在融合前后有很好的相关性，这说明了融合后的影像延续了融合前影像的空间分布特征，能够反映出不同类型的地物的ET差异。在图5（c）的散点图中出现了一个形似尾巴的分布区域，这代表的地物类型是水体，由于融合前的影像只能反映一天的蒸散量，通过变换的水体的月蒸散量集中在100 mm左右，融合后的影像反映了低分辨率的蒸散量一个月内变化和蒸散总量，其值在135—150 mm之间，因此在散点图上形成一个尾巴状的分布区域。这也说明了融合后的数据在不同地物类型上的分异特征明显。

4 结论与展望

ETWatch系统中的STARFM融合方法将MODIS的ET时间变化信息与TM的ET空间差异信息的有机结合，从而可以构建出高时空分辨率ET数据集，在时间上保留了高时间分辨率数据的时间变化趋势，空间上又反映了高空间分辨率数据的空间细节差异，STARFM融合后的日ET数据与融合前1 km 日ET数据的平均相对误差为1.75%，融合后的月ET数据与融合前1 km 月ET数据的平均相对误差为0.2%，STARFM融合方法提高了ET遥感监测的时空精细程度。

对于不同的地物类型，STARFM的融合效果有所不同，对于耕地，地势平坦，地表类型差异小，融合过程产生的差异比林地和城区相对较小。

STARFM实质上仍然是一种加权变换的方法，跟下垫面的复杂程度有关，如果是小块作物，或陆地与水体的交界处，不同地物产生的权重信息不一样，从而形成交界处产生过渡带的现象。因此需要发展一种处理不同地物交界带的融合方法。

高分辨率的时相分布对STARFM数据融合的结果有一定的影响，如果高低分辨率影像日期相距太远，随着时间的推移，地表特征发生了变化，尤其是与蒸散信息相关的植被覆盖和气象条件等的变化对融合结果会产生影响。融合过程不能完全表现出这些变化信息，融合后结果时刻（t_2）的MODIS数据与融合前时

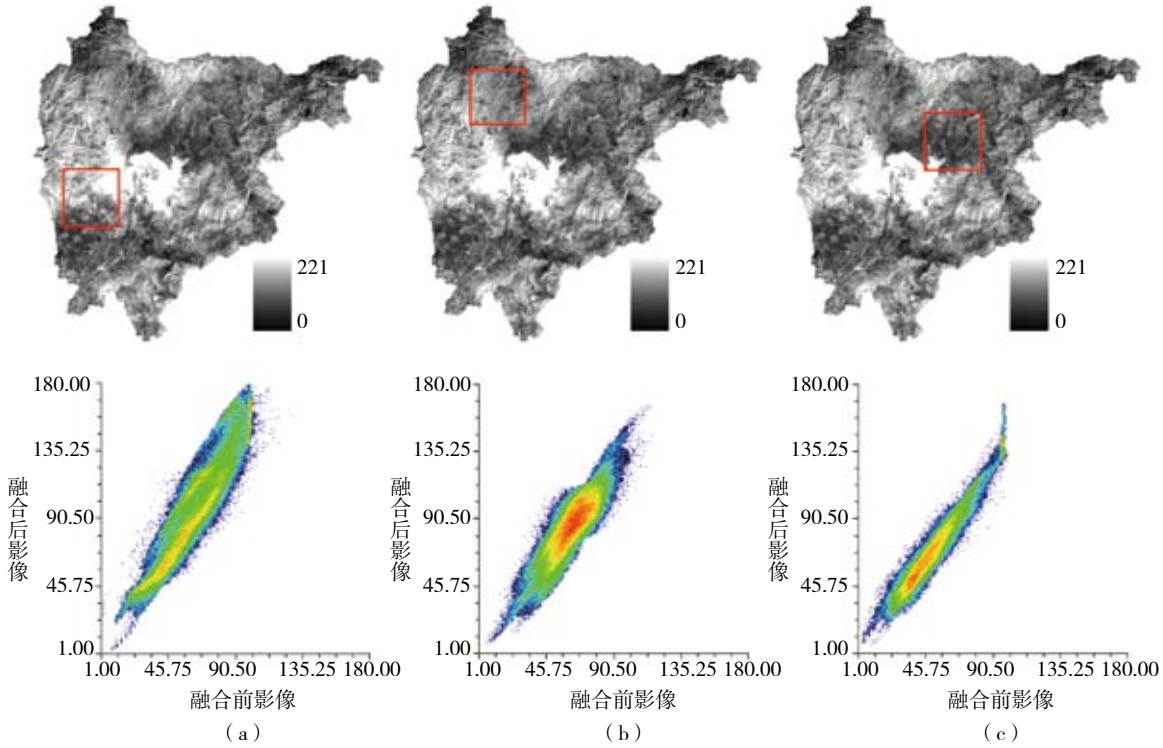

图5 不同土地利用类型ET融合结果的差异

(a) 耕地和水体；(b) 林地和裸地；(c) 水体、耕地和林地

刻（t_1）的TM数据和MODIS数据的日期差异越小，融合的结果越能体现高分辨率ET数据的空间分布特征，t_2和t_1时刻相差越大，如t_1到t_2时刻地表特征发生了较大的变化，融合结果产生的差异也相对越大。因此需要更多高分辨率数据参与到融合过程中。

目前可以获取30 m左右分辨率的数据包括TM、ETM、BJ-1、CBERS和HJ-1等，由于这些遥感数据来自不同的平台和传感器，不可避免的带有各自卫星和传感器的特点，产生了较大的不一致性，如何做好来自不同传感器的高分辨率影像的归一化和相互订正是做好数据融合的重要基础，是不同时空分辨率数据融合方法下一步的重要研究方向。

随着多源遥感数据的空前丰富，数据融合的需求也逐渐增多，未来的趋势是多源遥感数据的融合，根据问题的性质和模型的特点，选择什么环节进行融合，选择什么方法融合，是多源遥感数据融合的研究问题。

基于线性方法的融合保留了高分辨率数据的空间分布信息，但不能体现出ET数据变化的时间信息；非线性变换融合加强了ET数据变化的时间信息。

ETWatch系统中的STARFM融合方法综合考虑了ET数据的空间信息、光谱信息及时间变化信息，融合结果保留了高低分辨率数据的特征，适合于不同尺度下遥感ET数据的融合。

REFERENCES

Gao F, Masek J, Schwaller M and Hall H. 2006. On the blending of the Landsat and MODIS surface reflectance: Predicting daily Landsat surface reflectance. *IEEE Transactions on Geosciences and Remote Sensing*, **44**(8): 2207–2218

Gao X and Huete A R. 2002. Validation of MODIS land surface reflectance and vegetation indices with multi-scale high spatial resolution data. *Geosciences and Remote Sensing Symposium*, **2**: 533–535

Jia Y H, Li D R and Sun J B. 2000. Data Fusion Techniques for Multisources Remotely sensed Imagery. *Remote sensing technology and application*, **15**(1): 41–44

Jiang L P, Qin Z H and Xie W. 2006. Program splits window algorithm to retrieve land surface temperature for MODIS data using IDL. *Geomatics & Spatial Information Technology*, **29**(3): 114–117

Jin Z, Tian Q, Chen J M and Chen M. 2006. Spatial Scaling Between Leaf Area Index Maps of Different Resolutions. *Journal of Environmental Management*, **85**(3): 628–637

Jose A S, Juan C J and Leonardo P. 2004. Land surface temperature retrieval from LANDSAT TM5. *Remote Sensing of Environment*, **90**(4): 434–440

Kim G and Barros A P. 2002. Downscaling of remotely sensed soil

moisture with a modified fractal interpolation method using contraction mapping and ancillary data. *Remote Sensing of Environment*, **83**(3): 400–413

Mayaux P and Lambin E T. 1995. Estimation of tropical forest area from coarse spatial resolution data: a two-step correction function for proportional errors due to spatial aggregation. *Remote Sensing of Environment*, **53**(1): 1–15

Pohl C and Genderen J L. 1998. Multi-sensor image fusion in remote sensing: concepts, methods and applications. *International Journal of Remote Sensing*, **19**(5): 823–854

Steve Ackerman, Kathleen Strabala, Paul Menzel, Richard Frey, Chris Moeller, Liam Gumley, Bryan Baum, Suzanne Wetzel Seeman, and Hong Zhang. 2002. Discriminating Clear-Sky from Cloud with MODIS Algorithm Theoretical Basis Document (Mod35), Version 4.0

Sun J B, Liu J L and Li J. 1998. Multi-source remote sensing image data fusion. *Journal of remote sensing*, **2**(1): 47–50

Weng Y L and Tian Q J. 2003. Analysis and Evaluation of method on remote sensing data fusion. *Remote Sensing Information*, **37**(3): 49–53

Wu B F, Xiong J, Yan N N, Yang L D and Du X. 2008. ETWatch: Methodology of regional evapotranspiration monitoring with remote sensing. *Advances in Water Science*, **19**(5): 671–678

Wu B F and Shao J H. 2006. Temporal and spatial extension of evapotranspiration estimated from remote sensing. *Journal of Hydraulic Engineering*, **37**(3): 286–292

Wu J , Jiang H and Li Y H. 2008. Quality Assessment of RS image fusion. *Geomatics Technology and Equipment*, **10**(4): 9–11

Xiong J, Wu B F, Yan N N, Hu M G and Sun X M. 2008. Research on Temporal Reconstruction of Evapotranspiration by Using Remote Sensing. *Progress in Geography*, **27**(2): 53–59

Zhang W C, Zhong S and Hu S Y. 2008. Spatial scale transferring study on Leaf Area Index derived from remotely sensed data in the Heihe River Basin, *Chian*. *Acta Ecologica Sinica*, **28**(6): 2495–2502

附中文参考文献

贾永红，李德仁，孙家柄．2000．多源遥感影像数据融合．遥感技术与应用，**15**(1): 41–44

姜立鹏，覃志豪，谢雯．2006．MODIS数据地表温度反演分裂窗算法的IDL实现．测绘与空间地理信息，**29**(3): 114–117

孙家柄，刘继林．1998．多源遥感影像融合．遥感学报，**2**(1): 47–50

吴炳方，熊隽，闫娜娜，杨雷东，杜鑫．2008．基于遥感的区域蒸散量监测方法—ETWatch．水科学进展，**19**(5): 671–678

吴炳方，邵建华．2006．遥感估算蒸腾蒸发量的时空尺度推演方法及应用．水利学报，**37**(3): 286–292

翁永玲，田庆久．2003．遥感数据融合方法分析与评价综述．遥感信息，**37**(3): 49–53

武坚，江洪，李云虎．2008．遥感影像融合的质量评价探讨．测绘技术装备，**10**(4): 9–11

熊隽，吴炳方，闫娜娜，胡明罡，孙晓敏．2008．遥感蒸散模型的时间重建方法研究．地理科学进展，**27**(2): 53–59

张万昌，钟山，胡少英．2008．黑河流域叶面积指数（LAI）空间尺度转换．生态学报，**28**(6): 2495–2502